Journal of Zhejiang University SCIENCE A
ISSN 1673-565X (Print); ISSN 1862-1775 (Online)
www.zju.edu.cn/jzus; www.springerlink.com
E-mail: jzus@zju.edu.cn

Rotor broken bar fault diagnosis for induction motors based on double *PQ* transformation*

HUANG Jin, YANG Jia-qiang†‡, NIU Fa-liang

(*School of Electrical Engineering, Zhejiang University, Hangzhou 310027, China*)

†E-mail: yjq1998@163.com

Received Jan. 10, 2007; revision accepted Apr. 19, 2007

Abstract: A new rotor broken bar fault diagnosis method for induction motors based on the double *PQ* transformation is presented. By distinguishing the different patterns of the *PQ* components in the *PQ* plane, the rotor broken bar fault can be detected. The magnitude of power component directly resulted from rotor fault is used as the fault indicator and the distance between the point of no-load condition and the center of the ellipse as its normalization value. Based on these, the fault severity factor which is completely independent of the inertia and load level is defined. Moreover, a method to reliably discriminate between rotor faults and periodic load fluctuation is presented. Experimental results from a 4 kW induction motor demonstrated the validity of the proposed method.

Key words: *PQ* transformation, Fault diagnosis, Load fluctuation, Fault severity factor, Induction motors
doi:10.1631/jzus.2007.A1320 **Document code:** A **CLC number:** TM343

INTRODUCTION

Induction motors are widely used in modern industrial drives due to its robustness and low cost. However, the rotor bars cannot always be firmly fixed. The vibration of rotor bars will increase during the actual manufacturing process with the effect of strong electromagnetic and eccentric force when a motor is under a heavy load or starting and braking frequently. These will cause rotor bars to be cracked or broken, especially for large induction motors, such as the coal-transport motors in thermoelectric plant, etc. The fatigue stresses of the adjacent bars will increase if the motors with broken bars continue operating. It will aggravate the fault quickly and may cause rubbing between rotor and stator, and consequently damage to the stator core and windings. Hence, it is very important to diagnose rotor broken bar fault at their early stage, as an unscheduled machine downtime can upset deadlines and cause heavy financial losses.

For an induction motor with rotor broken bar fault, the harmonic components at frequencies described in Eq.(1) will appear in the stator current spectrum (Kliman *et al*., 1988; Filippetti *et al*., 1998; Han and Song, 2003; Marei *et al*., 2005; Bellini e*t al*., 2002; 2006; Luis *et al*., 2006):

$$f_{br}=(1\pm 2ks)f_s, \tag{1}$$

where f_s is the supply frequency, s is the slip of the motor, $k\in\mathbb{N}^*$. A commonly used approach for rotor broken bar diagnosis is based on the analysis of the stator current spectrum. Amplitude of the associated spectra component can be used to evaluate the fault severity. However, the slip for a typical induction motor under rated condition is small. It is even smaller under light-load or no-load conditions. This means that the fault characteristic frequency of $(1\pm 2s)f_s$ is very close to the supply frequency. As a result, they will always be submerged by the fundamental component. This will make the fault diagnosis even difficult (Cruz *et al*., 2003; Cupertino *et al*., 2004; Niu *et al*., 2005). It has become a bottleneck for

‡ Corresponding author
* Project (No. 50677060) supported by the National Natural Science Foundation of China

rotor broken bars fault diagnosis in induction motors.

In order to avoid the influence of the spectrum leakages of the fundamental component, Cardoso and Saraiva (1993) and Cruz and Cardoso (2000) proposed the Park vector and the extended Park vector methods, respectively. The former transforms the spectrum analysis into the recognition of graphics. But it just discriminates a circle from an ellipse, which is difficult at the inception of the rotor broken bars fault. The latter introduces some new frequency components due to the effect of the square operator. Despite these disadvantages, the authors developed a new diagnostic technique based on the multiple reference frames theory (Cruz *et al*., 2003; Cruz and Cardoso, 2004). However, a precise value of supply frequency must be given first, which is difficult when the supply quality is poor. Utilizing the modern signal processing techniques such as wavelet analysis, Hilbert-Huang transformation, etc., researchers tried to investigate the startup or breakdown process of the induction motors (Cupertino *et al*., 2004; Niu *et al*., 2005). However, these methods are not always valid. Moreover, the load fluctuation cannot be taken into account and the appropriate expression of the fault severity is not given.

In order to overcome this technique puzzle, a new method of rotor broken bar fault diagnosis for induction motors based on the double *PQ* transformation is presented in this paper. Detection of the rotor broken bar fault is realized and a fault severity factor which is completely independent of the inertia and load level of the induction motors is defined. The discrimination between rotor broken bar fault and periodic load fluctuation is also addressed at the end of the paper.

PQ TRANSFORMATION

Synchronous *dq*0 reference frame transformation method

The transformation matrix from the stationary three-phase *abc* to the synchronous $d_c q_c 0$ reference frame can be expressed as

$$\boldsymbol{C}_{d_c,q_c}^{a,b,c}=\sqrt{\frac{2}{3}}\begin{bmatrix}\cos\theta & \cos(\theta-2\pi/3) & \cos(\theta+2\pi/3)\\ -\sin\theta & -\sin(\theta-2\pi/3) & -\sin(\theta+2\pi/3)\end{bmatrix}, \tag{2}$$

where $\theta=\omega_s t+\theta_0$ is the angle between *d*-axis and *a*-axis, θ_0 is the angle at $t=0$ and $\omega_s=2\pi f_s$. For simplicity, the zero sequence components have been left out in this paper.

The fundamental positive sequence current components appear as constants in the *dq* current components. The frequencies of the fault feature components in Eq.(1) are transformed to $2ksf_s$. But the accurate supply frequency is very difficult to measure because it keeps fluctuating. If there is an error, Δf_s, between the actual frequency and the measured one, a component at frequency Δf_s will be introduced into the *dq* current components. On the other hand, because the rated slip is only approximately 0.5%~5% for induction motors, the fault feature frequency $2ksf_s$ is about 0.5~5 Hz for $k=1$. Therefore, the fault feature components will be mixed with the introduced component due to the error in the measured supply frequency, which makes reliable fault diagnosis difficult.

Definition of the *PQ* transformation

Ideally, the balanced supply voltage in the *abc* reference frame can be expressed as

$$\begin{cases}u_a=\sqrt{2}U\cos(\omega_s t),\\ u_b=\sqrt{2}U\cos(\omega_s t-2\pi/3),\\ u_c=\sqrt{2}U\cos(\omega_s t+2\pi/3),\end{cases} \tag{3}$$

where $\sqrt{2}U$ refers to the magnitude of the phase voltages. The stator currents can be written as

$$\begin{cases}i_a=\sqrt{2}I\cos(\omega_s t-\alpha_I),\\ i_b=\sqrt{2}I\cos(\omega_s t-\alpha_I-2\pi/3),\\ i_c=\sqrt{2}I\cos(\omega_s t-\alpha_I+2\pi/3),\end{cases} \tag{4}$$

for a healthy motor, where $\sqrt{2}I$ and α_I refer to the magnitude and the phase angle, respectively.

Obviously, the values of u_a, u_b and u_c can be used to substitute for the elements of the first row in Eq.(2). The elements of the second row in Eq.(2) can be obtained by performing Hilbert transformation on u_a, u_b and u_c respectively. Consequently, a new matrix $\hat{\boldsymbol{C}}_{d_c,q_c}^{a,b,c}$ is constructed as follows:

$$\hat{\boldsymbol{C}}_{d_c,q_c}^{a,b,c}=\begin{bmatrix}u_a & u_b & u_c\\ -H(u_a) & -H(u_b) & -H(u_c)\end{bmatrix}, \tag{5}$$

where H refers to the Hilbert operator. If the initial phase angle of the a-phase voltage is used as the angle between d- and a-axis, the relationship between Eq.(5) and Eq.(2) is

$$\hat{\boldsymbol{C}}_{d_c,q_c}^{a,b,c} \Big/ \boldsymbol{C}_{d_c,q_c}^{a,b,c} = \sqrt{3}U. \tag{6}$$

Then, performing the $dq0$ reference frame transformation on the stator currents based on $\hat{\boldsymbol{C}}_{d_c,q_c}^{a,b,c}$, the dq current components can be given by

$$\begin{bmatrix} i_d \\ i_q \end{bmatrix} = \hat{\boldsymbol{C}}_{d_c,q_c}^{a,b,c} \begin{bmatrix} i_a \\ i_b \\ i_c \end{bmatrix} = 3UI \begin{bmatrix} \cos\alpha_I \\ -\sin\alpha_I \end{bmatrix} = \begin{bmatrix} P \\ -Q \end{bmatrix}. \tag{7}$$

The active power P and the negative value of the reactive power Q are obtained from Eq.(7). Consequently, we define the transformation of the stator currents based on $\hat{\boldsymbol{C}}_{d_c,q_c}^{a,b,c}$ as the PQ transformation, which avoids calculation of the supply frequency. Exchanging the elements of the second and third column in Eq.(5), the counterclockwise PQ transformation matrix can be written as

$$\bar{\boldsymbol{C}}_{d_c,q_c}^{a,b,c} = \begin{bmatrix} u_a & u_c & u_b \\ -H(u_a) & -H(u_c) & -H(u_b) \end{bmatrix}. \tag{8}$$

Extraction of the fundamental positive sequence components of the supply voltage

The voltages of u_a, u_b and u_c in Eqs.(5) and (8) are the fundamental positive sequence components of the supply voltage. However, the supply voltage contains the negative sequence and the harmonics components. The PQ transformation matrix will become complicated (Lee *et al*., 2004). Therefore, the fundamental positive sequence components of the supply voltage must be extracted first in order to eliminate the unwanted harmonics in the PQ components.

A low-pass digital filter can be used to eliminate the high harmonics in the supply voltage. The filtered supply voltage which only comprises the positive and negative sequence fundamental components can be expressed as

$$\begin{cases} u_a = \sqrt{2}\left[U^+\cos(\omega_s t+\phi_u^+) + U^-\cos(\omega_s t+\phi_u^-)\right], \\ u_b = \sqrt{2}\left[U^+\cos(\omega_s t+\phi_u^+ - 2\pi/3) + \right. \\ \qquad \left. U^-\cos(\omega_s t+\phi_u^- + 2\pi/3)\right], \\ u_c = \sqrt{2}\left[U^+\cos(\omega_s t+\phi_u^+ + 2\pi/3) + \right. \\ \qquad \left. U^-\cos(\omega_s t+\phi_u^- - 2\pi/3)\right], \end{cases} \tag{9}$$

where $\sqrt{2}U^+$, $\sqrt{2}U^-$, ϕ_u^+ and ϕ_u^- refer to the magnitude and phase angle of the positive and negative sequence fundamental voltage components respectively. Then the $\alpha\beta$ voltage components can be achieved by

$$\begin{cases} v_\alpha = \sqrt{3}\left[U^+\cos(\omega_s t+\phi_u^+) + U^-\cos(\omega_s t+\phi_u^-)\right] \\ \quad = v_\alpha^+ + v_\alpha^-, \\ v_\beta = \sqrt{3}\left[U^+\sin(\omega_s t+\phi_u^+) - U^-\sin(\omega_s t+\phi_u^-)\right] \\ \quad = v_\beta^+ + v_\beta^-. \end{cases} \tag{10}$$

Performing Hilbert transformation on v_α and v_β in Eq.(10) respectively, the fundamental positive sequence components in the $\alpha\beta0$ reference frame can be calculated by

$$\begin{cases} v_\alpha^+ = [v_\alpha - H(v_\beta)]/2, \\ v_\beta^+ = [v_\beta + H(v_\alpha)]/2, \end{cases} \tag{11}$$

where v_α^+ and v_β^+ refer to the fundamental positive sequence components of the supply voltage in the $\alpha\beta0$ reference frame. Then, the fundamental positive sequence components of the supply voltage can be obtained through the reverse $\alpha\beta0$ reference frame transformation.

DIAGNOSIS OF ROTOR BROKEN BAR FAULT

Elimination of the negative sequence current components

The high order harmonics in the stator currents can be eliminated in a similar way with the one described earlier for the case of the supply voltages.

However, the negative sequence components in

the motor supply current will appear because of the inherent asymmetry of the induction motor and the asymmetrical supply voltages. This will result in 2nd order harmonic of the supply current in the *PQ* components, which can also make the rotor fault diagnosis difficult. Therefore, the negative sequence current components should be eliminated before the rotor broken bar fault diagnosis.

After being filtered with a low-pass filter, the stator currents for a healthy motor can be expressed as

$$\begin{cases} i_a = \sqrt{2}\left[I^+ \cos(\omega_s t - \phi_i^+) + I^- \cos(\omega_s t - \phi_i^-) \right], \\ i_b = \sqrt{2}\left[I^+ \cos(\omega_s t - \phi_i^+ - 2\pi/3) + \right. \\ \qquad \left. I^- \cos(\omega_s t - \phi_i^- + 2\pi/3) \right], \\ i_c = \sqrt{2}\left[I^+ \cos(\omega_s t - \phi_i^+ + 2\pi/3) + \right. \\ \qquad \left. I^- \cos(\omega_s t - \phi_i^- - 2\pi/3) \right], \end{cases} \tag{12}$$

where $\sqrt{2}I^+$, $\sqrt{2}I^-$, ϕ_i^+ and ϕ_i^- represent the magnitude and phase of the positive and negative sequence fundamental current components respectively. After performing the counterclockwise *PQ* transformation on the current components in Eq.(12), the *PQ* components include a component at twice the fundamental supply frequency and a DC component which should be filtered from them. The positive sequence current components can then be calculated through the reverse counterclockwise *PQ* transformation of the filtered *PQ* components.

Detection of the rotor broken bar fault

It can be concluded from Eq.(7) that both *PQ* components for a healthy motor are constant. If we define the *PQ* coordinate using the *P* and *Q* components as the coordinate axes, the locus of the *PQ* components for the healthy motor will correspond to a dot. But for the motor with rotor broken bar, its stator currents contain the new left and right side band components. And i_a' can be written as (Cruz *et al*., 2003)

$$\begin{aligned} i_a' = {} & \sqrt{2}I\cos(\omega_s t - \alpha_I) + \sqrt{2}I_l \cos[(1-2s)\omega_s t - \alpha_l] \\ & + \sqrt{2}I_r \cos[(1+2s)\omega_s t - \alpha_r], \end{aligned} \tag{13}$$

where $\sqrt{2}I_l$, $\sqrt{2}I_r$, α_l and α_r refer to the magnitude and phase of the left and right side band current components respectively. Performing *PQ* transformation on the current components described in Eq.(13), the *PQ* components can be calculated as follows:

$$\begin{aligned} \begin{bmatrix} P' \\ Q' \end{bmatrix} = \hat{\boldsymbol{C}}_{d_c,q_c}^{a,b,c} [i_a' \;\; i_b' \;\; i_c']^{\mathrm{T}} = \begin{bmatrix} P \\ -Q \end{bmatrix} + \\ 3U \begin{bmatrix} I_l \cos(2s\omega_s t + \alpha_l) + I_r \cos(2s\omega_s t - \alpha_r) \\ -I_l \sin(2s\omega_s t + \alpha_l) + I_r \sin(2s\omega_s t - \alpha_r) \end{bmatrix}. \end{aligned} \tag{14}$$

As can be concluded from Eq.(14), the *PQ* components contain a DC component plus an additional component at twice the rotor slip frequency when the rotor broken bar fault occurs. Obviously, the representation of the *PQ* components in the *PQ* plane is an elliptic pattern. The coordinates of the ellipse center are the DC values of the *PQ* components in the *PQ* plane and its major and minor axes are $3U(I_l+I_r)$ and $3U(I_l-I_r)$ respectively. Consequently, the rotor broken bar fault can be detected by recognition of the locus of the *PQ* components in the *PQ* plane.

The proposed fault diagnosis method, which combine counterclockwise and clockwise *PQ* transformations, is called the double *PQ* transformation.

Evaluation of rotor fault severity factor

Cruz *et al*.(2003) pointed out that the major axis of the ellipse can be used as the rotor fault indicator, and that the distance between the point of no-load condition and the center of the ellipse can be used as its normalization value. They also concluded that the fault severity factor, which is completely independent of the inertia and load level of the induction motors, can be obtained. However, based on the following analysis, the defined fault severity factor in (Cruz *et al*., 2003) is not completely independent of the inertia and load level.

Taking into account the speed oscillation effects, the side band current components for a rotor broken bar motor can be expressed as (Filippetti *et al*., 1998; Bellini *et al*., 2001).

$$\begin{cases} i_{a1} = \sqrt{2}I_1 \cos[(1-2s)\omega_s t - \alpha_{I_1}], \\ i_{a1}' = \sqrt{2}I_1' \sin[(1-2s)\omega_s t - \alpha_{I_1} - \phi_z], \\ i_{a2} = -\sqrt{2}I_2 \sin[(1+2s)\omega_s t - 2\alpha_\phi + \alpha_{I_1} - \phi_z], \end{cases} \tag{15}$$

where i_{a1} represents the first left side band component, which is directly derived from the rotor broken bar fault, i'_{a1} and i_{a2} are the left and right side band components derived from the consequent speed oscillation respectively. Performing PQ transformation on the current components in Eq.(14), the corresponding P and Q components can be given by

$$\begin{cases} P_1 = K_1 \cos(2s\omega_s t + \alpha_{I_1}), \\ P_1' = -K_1' \sin(2s\omega_s t + \alpha_{I_1} + \phi_z), \\ P_2 = -K_2 \sin(2s\omega_s t + \alpha_{I_1} - \phi_z - 2\alpha_\phi), \\ Q_1 = -K_1 \sin(2s\omega_s t + \alpha_{I_1}), \\ Q_1' = -K_1' \cos(2s\omega_s t + \alpha_{I_1} + \phi_z), \\ Q_2 = K_2 \cos(2s\omega_s t + \alpha_{I_1} - \phi_z - 2\alpha_\phi), \end{cases} \tag{16}$$

where $K_1=3UI_1$, $K_1'=3UI_1'$ and $K_2=3UI_2$.

Applying the principle of superposition, Eq.(16) can be rewritten as

$$\begin{cases} P^{\mathrm{F}} = (P_1 + P_1') + P_2 = P_{\mathrm{L}}^{\mathrm{F}} + P_{\mathrm{R}}^{\mathrm{F}}, \\ Q^{\mathrm{F}} = (Q_1 + Q_1') + Q_2 = Q_{\mathrm{L}}^{\mathrm{F}} + Q_{\mathrm{R}}^{\mathrm{F}}. \end{cases} \tag{17}$$

Substituting the variables in Eq.(17) with Eq.(16), the fault feature power components can be obtained as

$$\begin{cases} P_{\mathrm{L}}^{\mathrm{F}} = P_1 + P_1' = K_{\mathrm{L}} \cos(2s\omega_s t + \alpha_{I_1} + \beta), \\ P_{\mathrm{R}}^{\mathrm{F}} = P_2 = K_2 \cos(2s\omega_s t + \alpha_{I_1} - \phi_z - 2\alpha_\phi + \pi/2), \\ Q_{\mathrm{L}}^{\mathrm{F}} = Q_1 + Q_1' = -K_{\mathrm{L}} \sin(2s\omega_s t + \alpha_{I_1} + \beta), \\ Q_{\mathrm{R}}^{\mathrm{F}} = Q_2 = K_2 \sin(2s\omega_s t + \alpha_{I_1} - \phi_z - 2\alpha_\phi + \pi/2), \end{cases} \tag{18}$$

where superscript F refers to the feature power components derived from rotor broken bar fault, subscripts L and R refer to the left and right side band component respectively. And

$$\begin{cases} K_{\mathrm{L}} = \sqrt{(K_1 - K_1' \sin\phi_z)^2 + (K_1' \cos\phi_z)^2}, \\ \cos\beta = (K_1 - K_1' \sin\phi_z)/K_{\mathrm{L}}. \end{cases} \tag{19}$$

It can be seen from Eqs.(17) and (18) that the locus of P^{F} and Q^{F} in the PQ plane has elliptical pattern. And Eq.(17) can be transformed into the standard elliptical equation as

$$\begin{cases} P^{\mathrm{F}} = K_{\mathrm{L}} \cos[\theta_1 + (2\alpha_\phi + \phi_z + \beta - \pi/2)/2] + \\ \qquad K_2 \cos[\theta_1 - (2\alpha_\phi + \phi_z + \beta - \pi/2)/2], \\ Q^{\mathrm{F}} = -K_{\mathrm{L}} \sin[\theta_1 + (2\alpha_\phi + \phi_z + \beta - \pi/2)/2] + \\ \qquad K_2 \sin[\theta_1 - (2\alpha_\phi + \phi_z + \beta - \pi/2)/2], \end{cases} \tag{20}$$

where $\theta_1 = 2s\omega_s t + \alpha_{I_1} + (\beta - 2\alpha_\phi - \phi_z + \pi/2)/2$.

Using the power components to replace the current components, the fault severity factor δ can be rewritten as

$$\delta = (K_{\mathrm{L}} + K_2)/S, \tag{21}$$

where $S = \sqrt{(P - P_{\mathrm{o}})^2 + (Q - Q_{\mathrm{o}})^2}$ represents the load power component. The numerator represents the major axis of the ellipse and the denominator represents the distance between the point of (P,Q) whose coordinates are the DC values of the PQ components and the point $(P_{\mathrm{o}},Q_{\mathrm{o}})$ corresponding to the no-load condition of the motor in the PQ plane.

When the motor operates under the no-load condition, ϕ_z is close to 90°. As can be seen from Eqs.(16) and (17), P_1 has the reverse phase angle with P_1' and the same phase angle with $P_{\mathrm{R}}^{\mathrm{F}}$. Similarly, the same relationship lies in the Q-axis components. As the slip is very small for large induction motors, $1\pm 2s\cong 1$, i.e., $I_1'\approx I_2$ (Filippetti *et al*., 1998; Bellini *et al*., 2001). Therefore, the major axis of the ellipse follows

$$K_{\mathrm{L}} + K_2 \approx K_1. \tag{22}$$

In this condition, the fault severity factor δ, using the major axis of the ellipse as the fault indicator, is independent of the inertia and load of the motor. But ϕ_z will be decreased with the increase of the load level, which will result in

$$K_{\mathrm{L}} + K_2 > K_1. \tag{23}$$

With the increase of the load level, the calculated δ will be increased, as shown in Fig.1, which shows the relationship between δ and the power factor of the motor for several different values of K_1'/K_1.

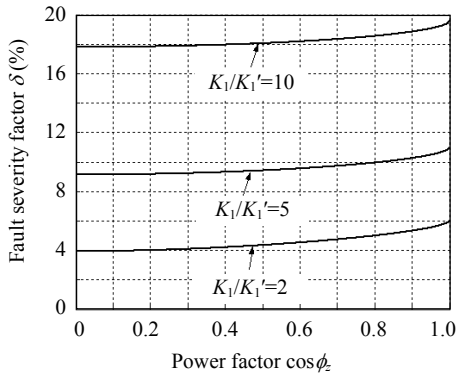

Fig.1 Fault severity factor vs power factor of the motor

According to the detailed discussion (Filippetti *et al*., 1998; Bellini *et al*., 2001), it can be concluded that

$$\frac{K_1}{K_1'}=\frac{8Js^2\omega_s Z}{3(1-2s)p^2\phi^2}, \tag{24}$$

where $Z=\sqrt{x^2+(r_s+r_r/s)^2}$ represents the equivalent circuit impedance, x represents the sum of the stator and rotor leakage reactance, r_s and r_r represent the stator and rotor resistance, respectively. Based on the above analysis, the law can be given as

$$\begin{cases} load\uparrow\rightarrow\cos\phi_z\uparrow\rightarrow s\uparrow\rightarrow K_1'/K_1\uparrow\rightarrow\delta\uparrow, \\ inertia(J)\uparrow\rightarrow K_1'/K_1\uparrow\rightarrow\delta\uparrow. \end{cases} \tag{25}$$

It can be concluded that, using the major axis of the ellipse as the fault indicator, the defined fault severity factor cannot be completely independent of the inertia and load of the motor. In order to get a more appropriate evaluation for δ, the power component corresponding to the first left-side-band current component, which is directly derived from the rotor broken bar fault, should be selected as the indicator. Thus, a new fault severity factor δ' is defined as

$$\delta'=K_1/S. \tag{26}$$

Calculation of the rotor fault indicator

In order to calculate the fault severity factor defined by Eq.(26), the magnitude K_1 of the power component directly derived from rotor broken bar fault should be calculated firstly. Performing Hilbert transformation on the second formula of Eq.(20), then adding it to the first one, the result can be obtained as

$$\begin{cases} P_L^F=[P^F+H(Q^F)]/2, \\ P_R^F=[P^F-H(Q^F)]/2. \end{cases} \tag{27}$$

Q_L^F and Q_R^F can be calculated in a similar way. The PQ components are thus decomposed into the left and right side band components which are respectively of $\boldsymbol{p}_L^F=\{P_L^F,Q_L^F\}$ and $\boldsymbol{p}_R^F=\{P_R^F,Q_R^F\}=\{P_2,Q_2\}$.

As can be seen from Eqs.(16) and (17), $\boldsymbol{p}_1'=\{P_1',Q_1'\}$ and $\boldsymbol{p}_R^F$, which are derived from the consequent speed oscillation, are approximately equal in magnitude and displaced by $2\alpha_\phi+2\phi_z$ in phase. Therefore, $\boldsymbol{p}_1'$ can be computed by shifting $\boldsymbol{p}_R^F$ backward by $2\alpha_\phi+2\phi_z$. Then, subtracting $\boldsymbol{p}_1'$ from $\boldsymbol{p}_L^F$, the feature components of $\boldsymbol{p}_1=\{P_1,Q_1\}$ can be directly derived from the rotor broken bar fault and its magnitude K_1 can be obtained.

DISCRIMINATION OF ROTOR BROKEN BAR FAULT AND LOAD FLUCTUATION

If the speed oscillation of $\Delta\omega$ is derived from the motor load fluctuation at frequency $s\omega_s$, the side band components of $(1\pm2s)f_s$ will also appear in the stator currents. Therefore, when the frequency of load fluctuation is close to the frequency of rotor fault feature components, their spectrum will be mixed with each other, which will cause error in the diagnostic results (Schoen and Habetler, 1995; 1997). Consequently, how to discriminate the rotor broken bar fault and the load fluctuation of the motor is a major problem.

According to (Filippetti *et al*., 1998; Bellini *et al*., 2001), if the load fluctuates at frequency of $s\omega_s$ for the healthy motor, the induced feature components in the stator current can be expressed as

$$\begin{cases} i_{a1}'=\sqrt{2}I_1'\sin[(1-2s)\omega_s t-\alpha_{I_1}-\phi_z], \\ i_{a2}=-\sqrt{2}I_2\sin[(1+2s)\omega_s t-2\alpha_\phi+\alpha_{I_1}-\phi_z]. \end{cases} \tag{28}$$

Similarly, performing PQ transformation on the currents components in Eq.(28), the results can be given by

$$\begin{cases} P^{\mathrm{T}} = P_1' + P_2 = P_{\mathrm{L}}^{\mathrm{T}} + P_{\mathrm{R}}^{\mathrm{T}}, \\ Q^{\mathrm{T}} = Q_1' + Q_2 = Q_{\mathrm{L}}^{\mathrm{T}} + Q_{\mathrm{R}}^{\mathrm{T}}, \end{cases} \tag{29}$$

where superscript T refers to the feature components derived from load fluctuation, subscripts L and R correspond to the left and right side band current components, respectively.

Substituting the variables in Eq.(29) with Eq.(16), Eq.(29) can be rewritten as

$$\begin{cases} P_{\mathrm{L}}^{\mathrm{T}} = P_1' = K_1' \cos(2s\omega_{\mathrm{s}}t + \alpha_{I_1} + \phi_z + \pi/2), \\ P_{\mathrm{R}}^{\mathrm{T}} = P_2 = K_2 \cos(2s\omega_{\mathrm{s}}t + \alpha_{I_1} - \phi_z - 2\alpha_\phi + \pi/2), \\ Q_{\mathrm{L}}^{\mathrm{T}} = Q_1' = -K_1' \sin(2s\omega_{\mathrm{s}}t + \alpha_{I_1} + \phi_z + \pi/2), \\ Q_{\mathrm{R}}^{\mathrm{T}} = Q_2 = K_2 \sin(2s\omega_{\mathrm{s}}t + \alpha_{I_1} - \phi_z - 2\alpha_\phi + \pi/2). \end{cases} \tag{30}$$

As can be seen from Eq.(30), the locus of P^{T} and Q^{T} is also an elliptical pattern in the PQ plane. And Eq.(29) can also be transformed to the standard elliptical equation as

$$\begin{cases} P^{\mathrm{T}} = K_1' \cos[\theta_2 + (\alpha_\phi + \phi_z)] + K_2 \cos[\theta_2 - (\alpha_\phi + \phi_z)], \\ Q^{\mathrm{T}} = -K_1' \sin[\theta_2 + (\alpha_\phi + \phi_z)] + K_2 \sin[\theta_2 - (\alpha_\phi + \phi_z)], \end{cases} \tag{31}$$

where $\theta_2 = 2s\omega_{\mathrm{s}}t + \alpha_{I_1} - \alpha_\phi + \pi/2$.

Ideally, discrimination of the rotor broken bar fault and load fluctuation can be realized by calculating δ'. According to Eq.(26) and the above discussion, δ' should be zero for the load fluctuating motor. However, it can be concluded from (Filippetti *et al*., 1998; Bellini *et al*., 2001) that $I_2 > I_1'$ due to the influence of the motor slip. Therefore, δ' is not zero, but a value related to the minor axis of the ellipse. The problem will become even more complicated when the frequency of the load fluctuation is non-sinusoidal. Consequently, more effective discrimination method should be investigated.

Defining the angle between the major axis of the ellipse and the P axis for the rotor broken bar and the load fluctuated motor as α_{F} and α_{T} respectively, the following results can be achieved based on Eq.(20) and Eq.(31), i.e.,

$$\begin{cases} \alpha_{\mathrm{F}} = \pi - (2\alpha_\phi + \phi_z + \beta - \pi/2)/2, \\ \alpha_{\mathrm{T}} = \pi - (\alpha_\phi + \phi_z). \end{cases} \tag{32}$$

$\phi_z \in (0,\pi/2)$ for a loaded induction motor and $\alpha_\phi \approx \pi/2$ because the stator resistance and leakage reactance are usually very small, therefore $\alpha_{\mathrm{T}} \in (0,\pi/2)$. It can be demonstrated from Eq.(19) that $\alpha_{\mathrm{F}} \in (\pi/2, 3\pi/4)$ when the inertia of the motor approaches some critical value (Filippetti *et al*., 1998; Bellini *et al*., 2001).

Consequently, the rotor broken bar fault and the load fluctuation can be discriminated by recognition of the orientation of the ellipse of the PQ components in the PQ plane. The ellipses of E_{F} and E_{T} for the rotor broken bar and load fluctuated motor are shown in Fig.2.

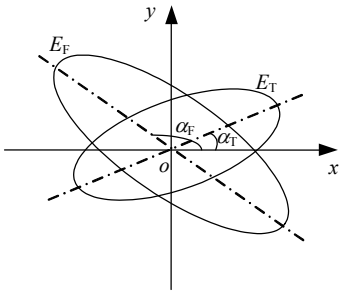

Fig.2 Ellipse for load fluctuated and rotor fault motor

The relationship between α_{F}, α_{T} and the motor power factor $\cos\phi_z$ for $I_1'/I_1=5$ is shown in Fig.3. They both increase with the motor load level, but satisfy $\alpha_{\mathrm{F}} \in (\pi/2, 3\pi/4)$ and $\alpha_{\mathrm{T}} \in (0,\pi/2)$ all along.

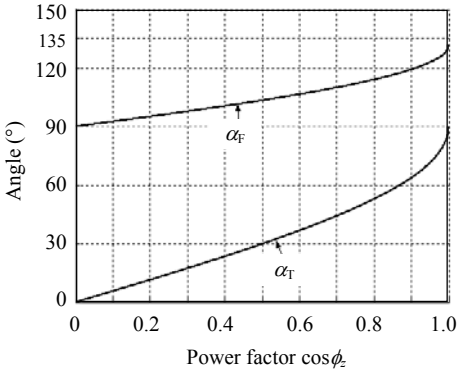

Fig.3 α_{F} and α_{T} vs the motor power factor when $I_1'/I_1=5$

EXPERIMENTAL RESULTS

Experimental system

In order to test the applicability of the proposed

diagnostic techniques for the diagnosis of rotor broken bars, a special test motor was used. It was a 4 kW, 380 V, 10 A, 50 Hz, 4 pole, 1400 r/min, 32 rotor bars induction motor. A set of additional cage rotors fabricated with the following faults, one rotor broken bar, two-adjacent rotor broken bars are used for test. The test motor is star-connected and without neutral line. A coaxial separately excited DC generator is used as the load of the test motor. The load oscillation of the induction motor is simulated by periodically changing the external resistance which is used as the load of the DC generator.

The terminal data u_{ab}, u_{cb}, i_a and i_c of the line-connected motor are acquired. The voltages and currents of the 3rd phase can be calculated by

$$i_b = -(i_a + i_c), \tag{33}$$

$$\begin{bmatrix} u_a \\ u_b \\ u_c \end{bmatrix} = \frac{1}{3}\begin{bmatrix} 1 & 0 & -1 \\ -1 & 1 & 0 \\ 0 & -1 & 1 \end{bmatrix}\begin{bmatrix} u_{ab} \\ u_{bc} \\ u_{ca} \end{bmatrix} = \frac{1}{3}\begin{bmatrix} 2u_{ab} - u_{cb} \\ -u_{ab} - u_{cb} \\ -u_{ab} + 2u_{cb} \end{bmatrix}. \tag{34}$$

The sample rate is 10 kHz and the software synchronization is adopted. A pre-filter whose cutoff frequency satisfies the Shannon sample law is used to avoid the collapse of high frequency components. The same low pass digital filter is used to filter the high-frequency components in the sample data.

Results and analysis

The *PQ* locus is shown in Fig.4 when the test motor is under the rated load condition. E_n, E_1 and E_2 are for the healthy as well as one and two adjacent rotor broken bars motor. E_n shows that the *PQ* components are both basically constant for the healthy motor. So their representation is a point in the *PQ* plane. But if the motor has rotor broken bar fault, the representation of its *PQ* components is an ellipse in the *PQ* plane. The major and minor axes for the two adjacent rotor broken bars motor are longer than those for the one rotor broken bar motor. This demonstrates that the fault is more serious, which agrees with the number of rotor broken bars. The ellipse centers are different, because the motor load had feeble variations during the 3 tests.

Using the magnitude of $\boldsymbol{p}_1$ and the major axis of the ellipses as the fault indicator respectively, Fig.5 shows the relationship between the fault severity factor and the motor load level. It can be concluded from the results presented in Fig.7, that the fault severity factor δ' defined in this paper is basically constant under different motor load levels. This demonstrates that it is completely independent of the inertia and load level. However, δ will increase with the increase of the motor load level, and is larger than δ' at the same motor load level, which also agrees with the theoretical analysis.

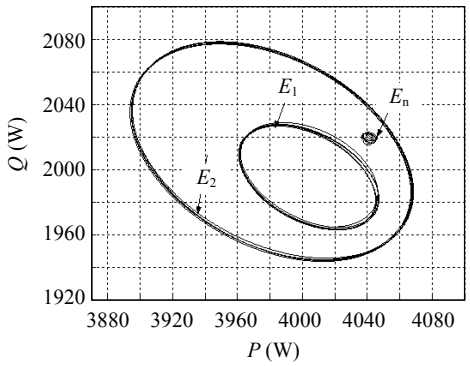

Fig.4 The *PQ* locus for the test motor

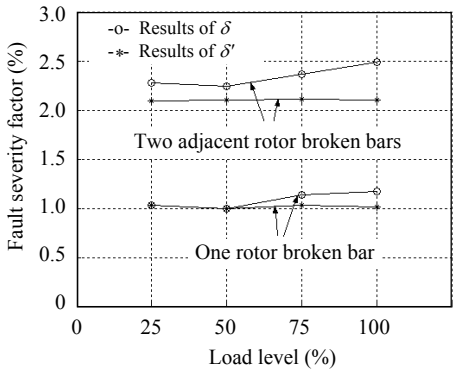

Fig.5 Fault severity factor vs load level of the rotor broken bar motor

Figs.6 and 7 show the locus of the *PQ* components for the two adjacent rotor broken bars and the load fluctuated motor when operated under half- and full-load respectively. As can be seen from Figs.6 and 7, the angle between the major axis of the ellipse and the *P* axis is larger than 90° for the motor with broken bar, but less than 90° for the load fluctuated motor. Therefore, the rotor broken bar fault and the load fluctuation can be easily discriminated based on the orientation of the ellipses. In both conditions, the angle between the major axis of the ellipse and the *P* axis increases with the motor load level. This also

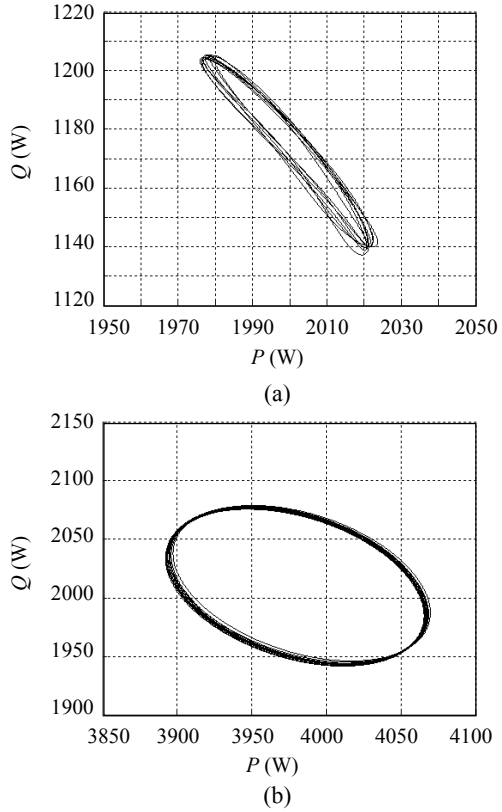

Fig.6 *PQ* of the two adjacent rotor broken bars motor
(a) Half-loaded; (b) Full-loaded

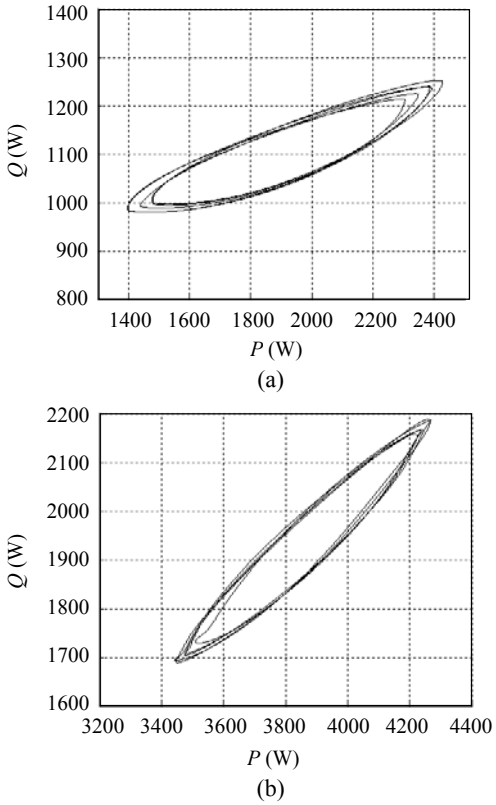

Fig.7 *PQ* of the load fluctuated motor
(a) Half-loaded; (b) Full-loaded

agrees with the theoretical results. Moreover, P_2/P_L will decrease with the increase of the motor load level, which leads to the decrease of the eccentricity of the ellipse for the rotor broken bar motor. This means the ellipse is more close to a circle with the increase of the motor load level. But P_1'/P_2 does not change significantly with the motor load level. The eccentricity of the ellipse for the load fluctuated motor also does not change significantly. Variations of the major and minor axes of the ellipse for the load fluctuating motor are feeble, because the manual adjustment of the resistance connected with the DC generator just cannot comply with the sine law.

CONCLUSION

This paper proposes a new rotor broken bar fault diagnosis method for induction motors based on the double *PQ* transformation. The rotor broken bar fault can be detected by recognition of the patterns of the *PQ* components in the *PQ* plane. The proposed method avoids the burden of computation of the supply frequency value, which is influenced by the quality of the supply. A new fault severity factor, which is completely independent of the motor inertia and load level, was defined by the justification of the choice of the fault indicator. Moreover, it has been shown that the presented scheme can also reliably discriminate between rotor broken bar fault and periodic load fluctuation of the induction motors.

References

Bellini, A., Filippetti, F., Franceschini, G., Tassoni, C., Kliman, G.B., 2001. Quantitative evaluation of induction motor broken bars by means of electrical signature analysis. *IEEE Trans. on Ind. Appl.*, **37**(5):1248-1255. [doi:10.1109/28.952499]

Bellini, A., Filippetti, F., Franceschini, G., Tassoni, C., Passaglia, R., Saottini, M., Tontini, G., Giovannini, M., Rossi, A., 2002. On-field experience with online diagnosis of large induction motors cage failures using MCSA. *IEEE Trans. on Ind. Appl.*, **38**(4):1045-1053. [doi:10.1109/TIA.2002.800591]

Bellini, A., Franceschini, G., Tassoni, C., 2006. Monitoring of induction machines by maximum covariance method for

frequency tracking. *IEEE Trans. on Ind. Appl.*, **42**(1): 69-78. [doi:10.1109/TIA.2005.861320]

Cardoso, A.J.M., Saraiva, E.S., 1993. Computer-aided detection of airgap eccentricity in operating three-phase induction motors by park's vector approach. *IEEE Trans. on Ind. Appl.*, **29**(5):897-901. [doi:10.1109/28.245712]

Cruz, S.M.A., Cardoso, A.J.M., 2000. Rotor cage fault diagnosis in three-phase induction motors by extended Park's vector approach. *Electric Machines and Power Systems*, **28**(3):289-299.

Cruz, S.M.A., Cardoso, A.J.M., Toliyat, H.A., 2003. Diagnosis of Stator, Rotor and Airgap Eccentricity Faults in Three-phase Induction Motors Based on the Multiple Reference Frames Theory. Conference Record of the 2003 IEEE Industry Applications Society Annual Meeting, p.1340-1346.

Cruz, S.M.A., Cardoso, A.J.M., 2004. Diagnosis of stator inter-turn short circuits in DTC induction motor drives. *IEEE Trans. on Ind. Appl.*, **40**(5):1349-1360. [doi:10.1109/TIA.2004.834012]

Cupertino, F., Vanna, E.D., Salvatore, L., Stasi, S., 2004. Analysis techniques for detection of IM broken rotor bars after supply disconnection. *IEEE Trans. on Ind. Appl.*, **40**(2):526-533. [doi:10.1109/TIA.2004.824432]

Filippetti, F., Franceschini, G., Tassoni, C., Vas, P., 1998. AI techniques in induction machines diagnosis including the speed ripple effect. *IEEE Trans. on Ind. Appl.*, **34**(1): 98-108. [doi:10.1109/28.658729]

Han, Y., Song, Y.H., 2003. Condition monitoring techniques for electrical equipment—a literature survey. *IEEE Trans. on Power Deli.*, **18**(1):4-13. [doi:10.1109/TPWRD.2002.801425]

Kliman, G.B., Koegl, R.A., Stein, J., Endicott, R.D., Madden, M.W., 1988. Noninvasive detection of broken rotor bars in operating induction motors. *IEEE Trans. on Energy Conv.*, **3**(4):873-879. [doi:10.1109/60.9364]

Lee, L.M., Lee, D.C., Seok, J.K., 2004. Control of series active power filters compensating for source voltage unbalance and current harmonics. *IEEE Trans. on Ind. Electr.*, **51**(1):132-139. [doi:10.1109/TIE.2003.822040]

Luis, A.P., Denis, F., Daniel, S.G., Libano, F.B., Sergio, H., 2006. Application of the Welch, Burg and MUSIC Methods to the Detection of Rotor Cage Faults of Induction Motors. Transmission & Distribution Conference and Exposition, p.1-6.

Marei, M.I., Abdel-Galil, T.K., El-Saadany, E.F., Salama, M.M.A., 2005. Hilbert transform based control algorithm of the DG interface for voltage flicker mitigation. *IEEE Trans. on Power Deli.*, **20**(2):1129-1133. [doi:10.1109/TPWRD.2004.843461]

Niu, F.L., Huang, J., Yang, J.Q., Chen, L.Y., Jin, H., 2005. Rotor broken-bar fault diagnosis of induction motor based on Hilbert-Huang transformation of the startup electromagnetic torque. *Proc. CSEE*, **25**(11):107-112 (in Chinese).

Schoen, R.R., Habetler, T.G., 1995. Effects of time-varying loads on rotor fault detection in induction machines. *IEEE Trans. on Ind. Appl.*, **31**(4):900-906. [doi:10.1109/28.395302]

Schoen, R.R., Habetler, T.G., 1997. Evaluation and implementation of a system to eliminate arbitrary load effects in current-based monitoring of induction machines. *IEEE Trans. on Ind. Appl.*, **33**(6):1571-1577. [doi:10.1109/28.649970]